Advances in Nano Research, *Vol. 18, No. 6 (2025) 585-597*
https://doi.org/10.12989/anr.2025.18.6.585

One pot solvothermal synthesis of Zr-MOF and DNA-encapsulated Zr-MOF for improved current density towards OER

Zohaib Ashraf[1], Mamoona Andleeb[1], Muhammad Sajjad[1], Muhammad Ibrahim[2], Sheereen Afaq[1], Wasif Mahmood Ahmad Malik[1,3], Abdul Ghafoor[1], Muhammad Ismail[1], Francis Verpoort[*4,5] and Adeel Hussain Chughtai[**1]

[1]*Institute of Chemical Sciences*, *Bahauddin Zakariya University*, *Multan (60800)*, *Pakistan*
[2]*Department of Biochemistry*, *Bahauddin Zakariya University*, *Multan (60800)*, *Pakistan*
[3]*Department of Chemistry*, *Emerson University*, *Multan (60000)*, *Pakistan*
[4]*Laboratory of Organometallics*, *Catalysis and Ordered Materials*, *State Key Laboratory of Advanced Technology for Materials Synthesis and Processing, Center for Chemical and Material Engineering*, *Wuhan University of Technology*, *Wuhan (430070)*, *China*
[5]*Joint Institute of Chemical Research (FFMiEN)*, *Peoples Friendship University of Russia*, *(RUDN University)*, *Moscow-117198*, *Russia*

(*Received September 13, 2024, Revised May 6, 2025, Accepted May 21, 2025*)

Abstract. The global energy crisis and environmental pollution requires an urgent shift to renewable energy sources. Electrochemical water splitting is an emerging and promising method to generate hydrogen which is clean and sustainable energy carrier. To facilitate the sluggish Oxygen Evolution Reaction (OER), contemporary society has been actively searching for an electrocatalyst that can be synthesized easily, exhibits remarkable catalytic activity and maintains extraordinary stability over time. In this paper, solvothermal method was used to synthesize a Zr-MOF and DNA encapsulated-MOF in context of making the best use of the synergistic behavior of the material. To further confirm the synthesized samples various characterization techniques like PXRD, SEM, BET and FT-IR were performed. The electrochemical results show that synthesized DNA encapsulated Zr-MOF have small Tafel value of 59 mV/dec, a lower value of onset potential of 1.49 V, a lower over potential value of 294 mV and had high electrochemical surface area of 411.25 cm^2. The Chronoamperometry test also shows the high structure stability of material over 50 hours. This work highlights the potential of Zr-MOF based materials as effective and robust catalyst for electrochemical water splitting to replace the electrocatalysts that are based on noble metals for energy conversion and storage.

Keywords: DNA; electrocatalyst; MOF; OER; water splitting

1. Introduction

Currently, the primary challenges confronting global society include environmental degradation, the energy crisis, and resulting economic concerns. By 2050, the global population is expected to rise by 26% to around 9.7 billion leading to a roughly 50% increase in the world's total primary energy consumption (Jones and Warner, 2016). There is an urgent need to develop more sustainable and efficient renewable energy sources. In order to secure a sustainable and environmentally aware future, we need to discover a renewable energy source to reduce our dependence on fossil fuel (Szeberényi *et al*. 2022).

Scientists proposed investigating an alternative energy source that is sustainable and environmentally friendly. Solar, tidal, wind, hydro energies and lithium-ion batteries were utilized to give abundant and cost-effective energy to humanity although each has its own limitations (Rahman *et al*. 2022). Researchers shifted their focus to chemical energy and discovered that hydrogen is an exceptionally attractive chemical energy source (Abdin *et al*. 2020).

Hydrogen is the most environment friendly and uncontaminated energy source with the capability to outperform all current sources in terms of effectiveness and accessibility (Ahmed Malik *et al*. 2022). It serves as an energy source for several reasons (Ghazi *et al*. 2022). It has a high energy level of around 142 MJ/kg which is significantly more than gasoline's 44 MJ/kg (Masuk *et al*. 2021). It is renewable, non-toxic, storable, and does not produce combustion-related greenhouse gas emissions due to its zero-carbon content. The cars using hydrogen as fuel can operate with maximum output because of its exceptional energy efficiency. The fuel cells which used hydrogen gas as fuel are two to three times more effective than combustion engines driven by petrol and do not have any negative side effects (Abdelkareem *et al*. 2021). It only generates warm air and water vapor and it can also expand in the transportation and electricity generation (Sazali, 2020). Although the hydrogen economy is projected to be the most favored sustainable energy option, most technologies for producing hydrogen are still in the early stages of being brought to market. Nowadays, fossil fuels are the primary source of large-scale hydrogen production in industry. Approximately 96% of the world's hydrogen

*Corresponding author, Mr.,
E-mail: francis@whut.edu.cn
**Co-corresponding author, Mr.,
E-mail: adeelhussain@bzu.edu.pk

ISSN: 2287-237X (Print), 2287-2388 (Online)

production arises from coal gas, steam reforming of oil and natural gas which goes against the aim of depending on renewable energy sources. To completely remove the need for fossil fuels, hydrogen should be generated from plentiful and clean sources using environmentally friendly methods (Megia *et al*. 2021).

Electrochemical water splitting converting power into storable hydrogen is a practical and effective method to address significant energy shortages and reduce greenhouse gas emissions (Hayat *et al*. 2023). Water comprises 70% of the Earth's surface, making it the most plentiful resource. The water-splitting technique can produce hydrogen without any environmental consequences by utilizing water as a feedstock that is renewable (Acar *et al*. 2016). Oxygen produced as a byproduct has no adverse environmental impacts and can increase the economic efficiency of the electrolysis process through many applications (Mohammadpour *et al*. 2021). Water splitting theoretically necessitates a thermodynamic Gibbs free enthalpy of 237.2 kJ mol^{-1} which corelate with a standard potential of 1.23 V comparative to reversible hydrogen electrode (Cavaliere 2023). This enables reaction to proceed in electrolyzer thermodynamically. The major problems to the extensive use of water in water splitting for producing hydrogen gas are the adverse thermodynamics and high value of over potential (Wang *et al*. 2015). Currently, just 4% of hydrogen production worldwide is generated using water electrolysis (Mergel *et al*. 2013).

Water splitting involves the oxygen and hydrogen evolution reaction which occur on anode and cathode correspondingly in a electrolyzer and these are considered as two crucial half-cell reactions (McHugh *et al*. 2020). Based on kinetic and thermodynamic studies, these reactions are slow processes that necessitate a high value of voltage (1.23 V) to proceed (Martinez *et al*. 2020). Metal oxides (Vedrine, 2017), metal selenides (Cai *et al*. 2021), metal tellurides (Gautam *et al*. 2023), metal sulphides (Barman and Nanda, 2016), metal phosphides (Kibsgaard *et al*. 2015), MOFs and other catalysts were utilized to reduce energy barriers of this process (Lamiel *et al*. 2023). Pt, Ru and Ir oxides exhibited enhanced electro-catalytic activity in overcoming energy hurdles of OER (Oxygen Evolution reaction) and HER (Hydrogen Evolution reaction) (Tian *et al*. 2021). However, since these catalysts were composed of noble metal elements that were not commercial for industrial application, the issue persisted. Due to their limited quantity, these metals were highly valued and not used on industrial scale (Habib *et al*. 2023). Efforts are underway to build a catalyst that can replace present noble metal catalysts and may exceed their catalytic activity and that catalyst should be abundant on Earth (Wang *et al*. 2015), environmentally friendly (Lu *et al*. 2021), durable (Shin *et al*. 2022) and cost-effective.

The porous nanostructure of catalyst would play a crucial role in exposure of active sites to the both electrolyte and substrate which is essential for attaining the high catalytic activity. Metal Organic Frameworks (MOFs) known for their well-organized structures seem particularly suitable for this purpose (Long and Yaghi 2009). Both MOFs and Metal Organic Polyhedras (MOPs) have attained a significance attraction in research world due to their exceptional properties. MOFs have built-in features of both meso-porous as well as micro-porous materials inside a single frame (Hou *et al*. 2020), excellent feature of long-lasting porosity (Zhang *et al*. 2020), high crystallinity (Amaro-Gahete *et al*. 2019), regular pore sizes (Wu *et al*. 2021), stable frame-work (Baburin *et al*. 2008), uniform and well-organized morphologies (Nandiyanto and Okuyama 2011), outstanding thermal stability (Liang *et al*. 2022), remarkably larger surface areas (Farha *et al*. 2012), tunable pore size (Bonnett *et al*. 2020), enhanced pore dimensionality (98 Å) (Deng *et al*. 2012) with lesser density of 0.13 g cm^{-3} (Furukawa *et al*. 2011), flexible host-guest interactivity (D. Gao *et al*. 2021) and functionality (Kim and Hong 2021).

MOFs are a distinctive category of very porous compounds known for their exceptional long-range organization and crystallinity (Bennett and Cheetham, 2014). They are composed of organic linkers and metal ions (Yuan *et al*. 2015). MOFs have found their effectiveness in wide array of that include in adsorption (Dhaka *et al*. 2019), as sensors (Gao *et al*. 2021), in gas storage (Cai *et al*. 2021), in gas separation (Rodenas *et al*. 2015), in pesticides assay (Shi *et al*. 2023), in drugs loading (Falsafi *et al*. 2021), photo-catalytic reduction of Carbon dioxide (CO_2) (Gulati *et al*. 2023), in electrochemical application (Ding *et al*. 2019) and in inquisitory the alternate source for energy production. In their pure form, MOFs can be applied in a wide range of sectors.

Many MOFs have been utilized in electrochemical water splitting because of their inherent characteristics like as extensive surface areas (Abdelkareem *et al*. 2021), pore designs (Ding *et al*. 2019), flexible chemical components (Nemiwal *et al*. 2021) and various topologies (Cai *et al*. 2021). Moreover, the features of MOFs can be enhanced by adding other functional elements including metal compounds (Cui *et al*. 2016), biopolymers (Nadar *et al*. 2019), carbon nanotubes (CNTs) (Wang *et al*. 2015), polyoxometalates (POMs) (Miras *et al*. 2014) and other conductive substances to create MOF/substrates or guests@MOFs. Enhanced electrochemical results in electrolysis can be attained by increasing the number of porous active sites and enhancing conduction through different functionalization. Moreover, the Metal Organic based framework tolerates for molecular and atomic rearrangement during pyrolysis, enhancing its versatility and effectiveness (Wang and Astruc 2019). Derivatives of MOFs that undergo pyrolysis exhibit improved features such high stability, large surface area, high conductivity, porosity and catalytic activity, making them highly efficient for water splitting (Abdin *et al*. 2020). Over the past five years, various materials based on MOFs and their derivatives have been analyzed that were used as electrocatalyst.

Interactions of MOFs and biopolymers occur in various important areas (El Hankari *et al*. 2019). Due to their high biocompatibility, adjustable structure and high loading ability, MOFs have shown extensive usage in biological application and interactions between lipids, nucleic acids, peptides and MOF make them versatile in different

applications (Morris *et al*. 2014, Peng *et al*. 2020, Sava Gallis *et al*. 2022). From these, Deoxyribonucleic acid (DNA) has become a significant molecule in nanomaterials because of its accurate base-pairing properties and customizable sequence (Abdelkareem *et al*. 2021). Compared to MOFs which consist of several metal clusters or ions and atoms capable of coordinating with different chemical groups, DNA may provide a wide range of chemical groups through its base with a deoxy ribose sugar and phosphate group backbone. Interactions between MOF and Nucleic acid can be strengthened due to the formation of chemical bonds between metal clusters in MOFs and different chemical sites in nucleic acids. MOFs can adsorb DNA via hydrogen-bonding, electrostatic, π-stacking and coordination interactions (Wang *et al*. 2017). Zr-O-P bonds enhance the collaboration between Zr-based MOFs (Zr-MOF) and DNA which is controlled by a phosphate-induced site-occupying effect. DNA can stabilize MOFs by encapsulating the MOF structure in a protective shell to prevent aggregation or structural breakdown. This could lead to catalysts with increased durability (Zhang *et al*. 2021). MOFs often possess a substantial surface area which is beneficial for catalyzing reactions. The extensive surface area of DNA along with its ability to interact with water and facilitate reaction site can be utilized in DNA-MOF (Wu *et al*. 2020). Electron transfer is a vital step in the catalytic process of water splitting and DNA can be used to assist in this process (Karthick *et al*. 2020). DNA's non-toxic and biocompatible nature makes it potentially valuable in applications like water splitting systems (Dash *et al*. 2011).

MOF-801 is constructed of zirconium metal clusters and fumarate acid linkers. (Rameesha *et al*. 2024) MOF-801 is the smallest component of Zr-MOFs having a face-centered cubic close-packing (fcu) topology and formula of $Zr_6O_4(OH)_4(fumarate)_6$ (Furukawa *et al*. 2014). It was first reported in 2012 and has a topology similar to UiO-66. Its synthesis involved reacting $ZrCl_4$ with fumaric acid using solvothermal process and in the presence of modulator formic acid (Wißmann *et al*. 2012). Since its initial discovery, there has been a prominent increase in research interest surrounding MOF-801.The Secondary building Units (SBUs) is a zirconium oxide $[Zr_6(\mu_3\text{-}O)_4(\mu_3\text{-}OH)_4]$ octahedral group which comprise six Zirconium ions positioned at vertices of six polyhedron of the octahedron bounded through eight μ_3-oxygens. These eight equal faces of octahedron are consecutively topped by four μ_3-Oxygen groups and by four μ_3-OH. These Secondary sub units are interconnected by organic ligands making a network topology of 'fcu' (face centered cubic) type where every secondary sub unit is attached to twelve carboxylates (coo^{-1}) clusters from twelve different ligands.

In present work, we synthesized MOF-801 (Zr-MOF) by utilizing fumaric acid as a ligand and zirconium dichloride oxide octahydrate. DNAs were included into the MOF to prepare the DNA encapsulated DNA encapsulated Zr-MOF. The materials we studied showed excellent OER performance in alkaline conditions because of the synergistic effect of DNA encapsulated Zr-MOF. The DNA-based metal-organic framework material on nickel foam exhibited a lower onset potential of 1.49 V vs RHE (Reversible Hydrogen Electrode) and a lower overpotential value of 294 mV at a 10 $mAcm^{-2}$ standard current density. Moreover, the DNA encapsulated material exhibited minimum charge transfer resistance and maximum chrono-stability in chronoamperometry testing.

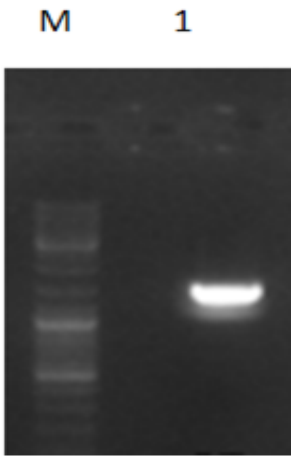

Fig. 1 Electrophoretic patterns of DNA of rhizobacteria (M = 1 Kb DNA marker/ladder. Lane 1DNA bands of rhizobacteria)

2. Experimental

2.1 Materials and physical measurements

$ZrOCl_2$ (Zirconium oxydichloride, purity 99.5%), fumaric acid (Merck, purity 98%), ethanol (C_2H_5OH), formic acid and nickel foam (Ni, Shanghai Co, purity95%) were purchased from Alfa Acer and Sigma-Aldrich and utilized without modifications. Deionized water from a Millipore system was used in all experiments. Powder X-ray Diffraction (PXRD) was measured employing Empyrean utensil from the PANalytical by engaging monochromatic Cu Kα under ambient conditions. Fourier Transform Infrared Spectroscopy (FTIR) analysis of prepared samples was done on PerkinElmer Spectrum One spectrometer. Elemental composition was achieved on the Vario EL cube. Scanning electron microscopy (SEM) images were executed on JEOL (JSM-5610LV). Porosity measurements were perceived with N_2 sorption isotherms on the Micromeritics instrument (ASAP 2020) at 77 K. Before Brunauer-Emmett-Teller (BET) analysis, samples were activated by solvent exchange method and were degassed overnight at 150 °C. Electrochemical studies were conducted using a computer-controlled AUTOLAB Potentiostat (PGSTAT-204).

2.2 Extraction of DNA

To extract DNA, we cultivate 1-3 mL of bacterial culture overnight to collect bacterial DNA. To prevent contamination, the culture must be completely separated from the supernatant by careful centrifugation at 6,000 rpm for two minutes. The bacterial pellet was disrupted and subsequently mixed with 100 µL of buffer R1. The 20 µL of

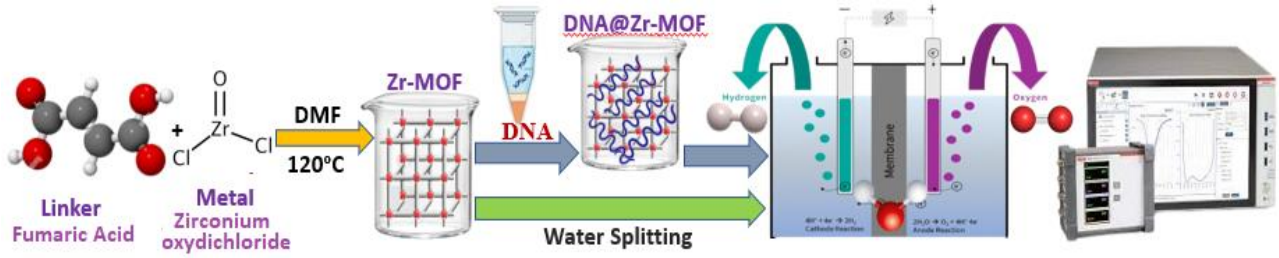

Scheme 1 Schematic representation for synthesis of Zr-MOF and DNA encapsulated Zr-MOF and their application as an electro-catalysts for water splitting.

lysozyme (50 mg/mL) was added to Gram-positive bacteria and the mixture was centrifuged to form a pellet after incubated at 37 °C for three minutes. Afterward, 20 µL of Proteinase K was added to bacterial pellet which was previously suspended in 180 µL of Buffer R2. Then, this mixture was incubated for 20 minutes at 60 °C. Then, mixture was added with Ribouclease (RNAase) at a concentration of 20 mg/mL and again incubated for about twenty minutes at 37 °C temperature. The DNA was purified after a comprehensive cleaning procedure and assessed for purity through a sequence of washing processes. DNA was stored in eppendorf at -20 °C**.** To verify the effectiveness of the extraction, DNA was examined on 1% agarose gel treated with ethidium bromide. 16S ribosomal Ribonucleic acid (RNA) gene was amplified by using universal primer in PCR and gel image of 16S ribosomal gene is depicted in Fig. 1 along with 1kb DNA ladder. Quantity and purity of the sample were determined using a spectrophotometer and the 260/280 ratio. This technique ensures dependable outcomes for various downstream applications due to its precision and consistency.

2.3 Preparation of Zr-MOF

Zr-MOF (MOF-801) using a single linker and zirconium metal source was prepared by solvothermal method with minor changes in previously reported procedure (Jahan *et al*. 2022, Lee *et al*. 2022). 0.7 mmol of fumeric acid (0.0812 grams) was added a Teflon carrier having 15 mL of N,N-dimethylformamide (DMF). A clear and uniform solution was obtained by constantly stirring the above solution on the stirring plate until the fumaric acid had dissolved. Then, 0.7 mmol of zirconium dichloride oxide octahydrate (0.2254 grams) was added along with 15 mL of formic acid in above solution (Scheme 1). Teflon was placed in auto clave and heated in oven at 120 ºC for approximately 24 hours. After the synthesis was completed, the autoclave having Teflon inside was cooled at room temperature. Finally, product was filtered and then washed three times with 10 mL DMF and dried at 100 ºC. The dried sample was used for characterization and electrochemical water splitting.

2.4 Preparation of DNA encapsulated Zr-MOF

In order to make the DNA encapsulated Zr-MOF, 300 milligrams of Zr-MOF were added to 4.5 milliliters of extracted DNA (suspension in eluting buffer) (Scheme 1). The mixture was then sonicated at 25 ºC for seven hours. After that, it was centrifuged at 25 °C for five minutes at 10,000 revolutions per minute (to remove the free DNA) until a pellet formed at the base of the tube. After collecting the supernatant, we dried the material. Once dried, it was preserved for further characterization and subjected to water splitting experiments.

2.5 Electrode preparation

For electrochemical study, a standard three-electrode system having a working electrode made of nickel foam (NF), the counter electrode made of Pt wire and the reference electrode of (Ag/AgCl) were used. The NF substrate was cut into 1 cm by 1 cm pieces and then underwent multiple cleaning procedures. The nickel foam pieces underwent ultrasonic treatment for 15 minutes in four separate solutions ethanol, de-ionized water, acetone and 2 M HCl. The NF pieces were then warmed at 60 °C for 30 minutes to remove moisture. We prepared a homogenous catalyst ink by finely grinding 1.5 mg of the synthesized materials and added 100 µL of de-ionized water. The catalyst ink underwent ultrasonic treatment for one hour. The catalyst ink was applied on the dried and cleaned NF by the drop-casting method. Precisely, 10 µL of the catalytic ink was applied to the chosen area of the NF components and dried at room temperature. Then, dried loaded NF fragments were utilized to examine the Oxygen Evolution Reaction (OER).

3. Results and discussion

3.1 Material characterization

Numerous techniques were used to characterize Zr-MOF and DNA encapsulated Zr-MOF. According to powder XRD, Zr-MOF and DNA encapsulated Zr-MOF have identical structure in good agreement with earlier described data for the MOF-801 suggesting the successful synthesis of Zr-MOF (Fig. 2). The PXRD pattern reveals two main peaks of Zr-MOF at 8.5◦ and 9.9◦ two theta that match to the planes (111) and (200) respectively (Aghajani Hashjin *et al*. 2023). These two sharp and highly intense peaks demonstrate that synthesized Zr-MOF has a high order of crystallinity. All the peaks in revealed pattern are efficaciously indexed which specifies the synthesis of the

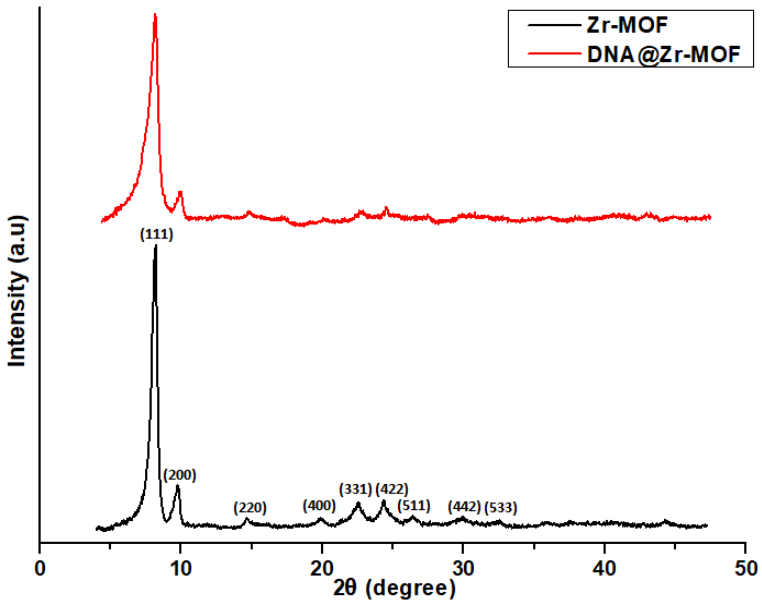

Fig. 2 XRD patterns of Zr-MOF

distinct structure of Zr-MOF by its space group of *Pn*-3 (#201) (Butova *et al*. 2021). The crystallite sizes of synthesized powder Zr-MOF are in the range from 17 nm to 29 nm for these two main peaks, (111) and (200) planes correspondingly and also in accordance with particle size calculated via SEM micrographs. The crystal sizes are calculated using Scherrer equation, $\beta = k\lambda / L\cos\theta$ where, θ is Bragg angle, k = 0.9, λ = 1.5406 Å, L is the crystalline size in angstroms (Å) and β denotes FWHM (Full-Width at the Half-Maximum) of diffraction peak measured in the radians.

A diffractogram of DNA encapsulated Zr-MOF exhibit distinctive peaks of Zr-MOF and its MOF-801 family at 8.5° and 9.9° indicating that DNA *in situ* does not interfere with the Zr-MOF synthesis. It can be perceived from the PXRD results that both Zr-MOF and DNA encapsulated Zr-MOF have alike PXRD pattern that completely identical with MOF-801. Though, it can be perceived that comparative intensity of PXRD peaks of DNA encapsulated Zr-MOF are lower related with Zr-MOF. The diffraction peaks of the DNA encapsulated Zr-MOF are in good agreement with the prepared Zr-MOF which displays well-defined Zr-MOF units in the material suggesting that the presence of DNA did not hinder the crystallization of the Zr-MOF structure and the DNA encapsulated Zr-MOF retained the structure of Zr-MOFs. The PXRD confirm that DNA encapsulation occurs through metal phosphate interaction preserving the porosity and structural integrity of Zr-MOF.

The FTIR spectra of DNA, Fumaric acid, Zr-MOF and the DNA encapsulated Zr-MOF are shown in Fig. 3. The spectral data of DNA of bacterial specie was documented in regions between 4000 and 400 cm^{-1}. Three distinct areas have been familiar in FTIR spectra including 1250-800 cm^{-1}, 1500-1250 cm^{-1} and 1800-1500 cm^{-1}. In our spectrum, a broad peak around 3298 cm^{-1} was owing to – stretching vibration of NH or O-H (Francioso *et al*. 2010) of DNA nitrogen bases pyrimidine and purine ring. While a strident intense peak at 1638 cm^{-1} was due to existence of carbonyl in amide I band (Liu *et al*. 2016). The region from 1515-1650 cm^{-1} assigned to the exocyclic bending of $-NH_2$ and C=C, C=N, C=O stretching in DNA bases. A band can be also predictable as a high frequency at 1085 cm^{-1} and another band 1245 cm^{-1} correspond to symmetric and a-symmetric stretching vibration of phosphate groups (PO^{2-}) (Mady *et al*. 2011) of the phosphor-di-ester-deoxyribose backbone. The small bands in region from 1164 to 1085 cm^{-1} and a sharp band at 1045 cm^{-1} were due to backbone from the C–O stretch and vibration of a sugar phosphate backbone respectively (Doorley *et al*. 2009). The region between 1000–800 cm^{-1} are assigned to the diverse sugar-phosphate backbone vibrations and nucleic acid S- and N-type of sugar puckering (Banyay *et al*. 2003).

A small intensity broad peak at 3430 cm^{-1} of MOF-801 can be credited to stretching vibration of hydroxyl group. Fumaric has a sharp highly intense peak at 1747 cm^{-1} due to carbonyl group stretching. The band at 1248 cm^{-1} could be allocated to C-O vibration. The presence of a number of bands in region 1002-670 cm^{-1} indicates rocking vibration of =CH group (Du *et al*. 2016).

The assignment of observed FTIR peaks in prepared Zr-MOF is effectively done rendering to conforming distinguishing peaks of MOF-801 (Aghajani Hashjin *et al*. 2023). Absorption bands at 1367 cm^{-1} and 1539 cm^{-1} are due to symmetric and asymmetric stretching of fumaric acid carboxylic group correspondingly (Fig. 3). The presence of these two significant peaks is ascribed to extended conjugate π-bonds of carboxylate group, originating from the carboxyl anion. This leads to the both oxygen atoms being equivalent resulting in symmetrical distribution of the electron cloud density between them. The two prominent bands at 478 and 644 cm^{-1} could be credited to Zr-O-C stretching and vibration of $Zr_6(OH)_4O_4$ cluster, correspondingly (Butova *et al*. 2020). Furthermore, the peaks in region from 900-700

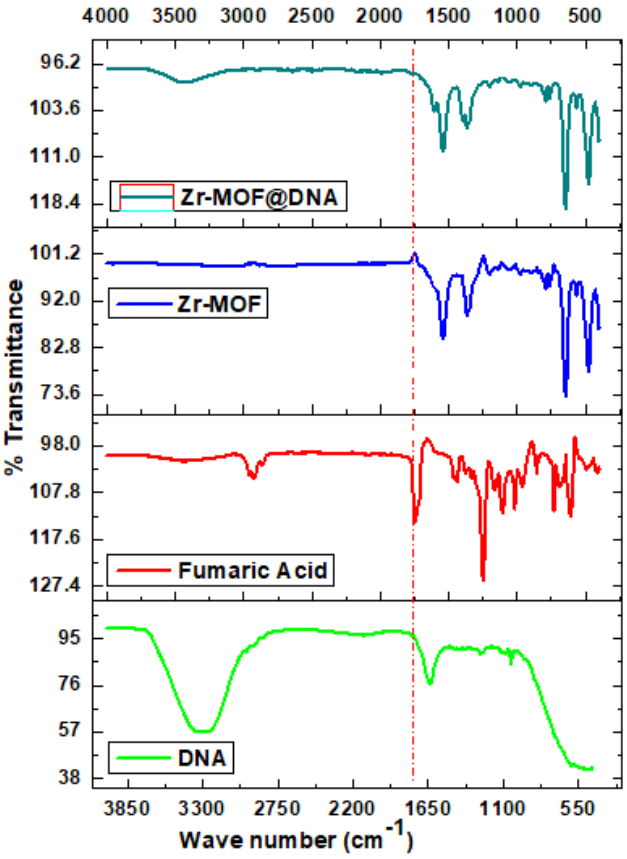

Fig. 3 FTIR spectra of (a) DNA (b) Fumaric Acid (Linker) (c) Zr-MOF (d) DNA encapsulated Zr-MOF

cm^{-1} (791 cm^{-1}, 891 cm^{-1} and 974 cm^{-1}) are given to -C-H bending vibration of carboxylic acid group of fumaric acid.

FTIR was also used to interpret fingerprint of DNA encapsulated Zr-MOF and the resultant spectra is presented in Fig. 3. A small broad peak at 3440 cm^{-1} (3680-3240) can be recognized to O-H or -NH groups stretching of DNA nitrogen bases. But it can also be detected that comparative intensity of some peaks in DNA encapsulated Zr-MOF are lower compared to Zr-MOF.

The enduring permeability of Zr-MOF and its (DNA encapsulated Zr-MOF) were confirmed at 77 K using its N_2 sorption isotherm. For activation, the Zr-MOF and DNA encapsulated Zr-MOF were soaked in methanol for 3 days and then in dichloromethane for 3 days. They were then dried at room temperature for 1 hour to prepare activated samples for analysis. The N_2 sorption isotherm of the MOF and its DNA@MOF showed a type II with pore condensation and distinctive adsorption-desorption hysteresis as depicted in Fig. 4. The results indicate the presence of mesopores in DNA encapsulated Zr-MOF with a maximum N_2 absorption of 350 cm^3/g. The BET surface area observed was 74.2800 ± 3.2718 m^2/g and the Langmuir surface area was 81.12 m^2/g which was higher than that of Zr-MOF with 64.7525 ± 3.1234 m^2/g (BET surface area) and 71.15 m^2/g (Langmuir surface area). The DNA encapsulated Zr-MOF has pore volume of 0.54 cm^3/g and pore diameter of 29.22 nm which are larger than the MOF (pore volume of 0.43 cm^3/g and

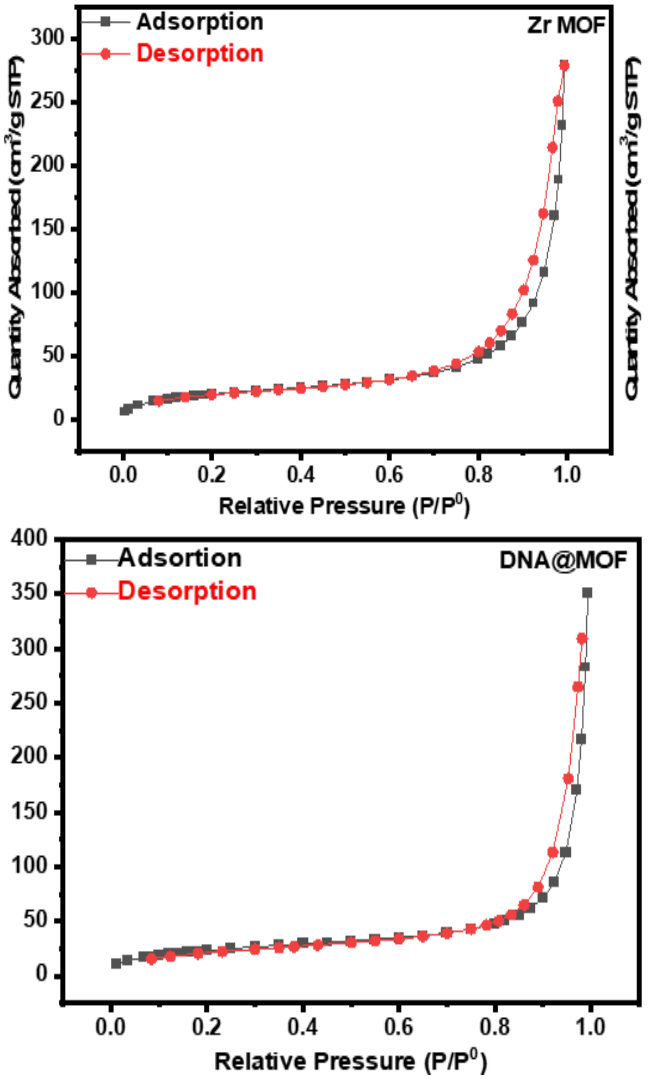

Fig. 4 Nitrogen sorption isotherm Zr-MOF and DNA encapsulated Zr-MOF

pore diameter of 26.66 nm). The DNA encapsulated Zr-MOF material's large pore volume and higher BET surface area are indicating its suitability for electrochemical applications.

3.2 Electro-catalytic OER

MOFs being distinctive catalysts have a proportion of prospective, mainly in the essential electro-catalysis. The coordinately unsaturated metal sites (Lewis's acid centers of the CUSs) and triggered functional groups on organic ligands (basic or acidic sites) are key active catalytic sites characteristically present in the MOFs. Electronic arrangement of the metallic components which can be influenced by the coordinated linkers has been shown an effectual slant to modify catalytic performance of the MOFs (Abazari *et al*. 2022, Pan *et al*. 2024, Wu *et al*. 2024).

Commonly, the metal center is contemplated as electro-catalytic active site in the MOF framework. The electro-catalytic activity towards the water splitting must be expressively prejudiced by the organic linker for MOFs.

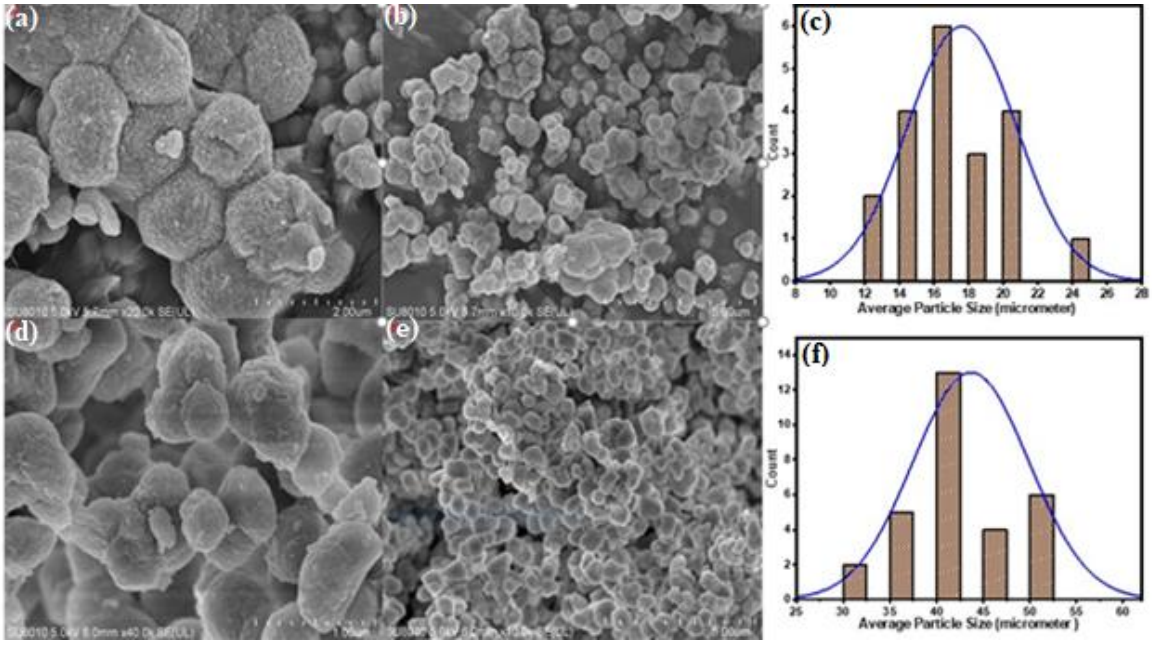

Fig. 5 SEM micrographs with corresponding insets revealing enlarged view Zr-MOF (a-b) and DNA encapsulated Zr-MOF d-e). Average particle sizes of Zr-MOF (c) and DNA@Zr-MOF (f)

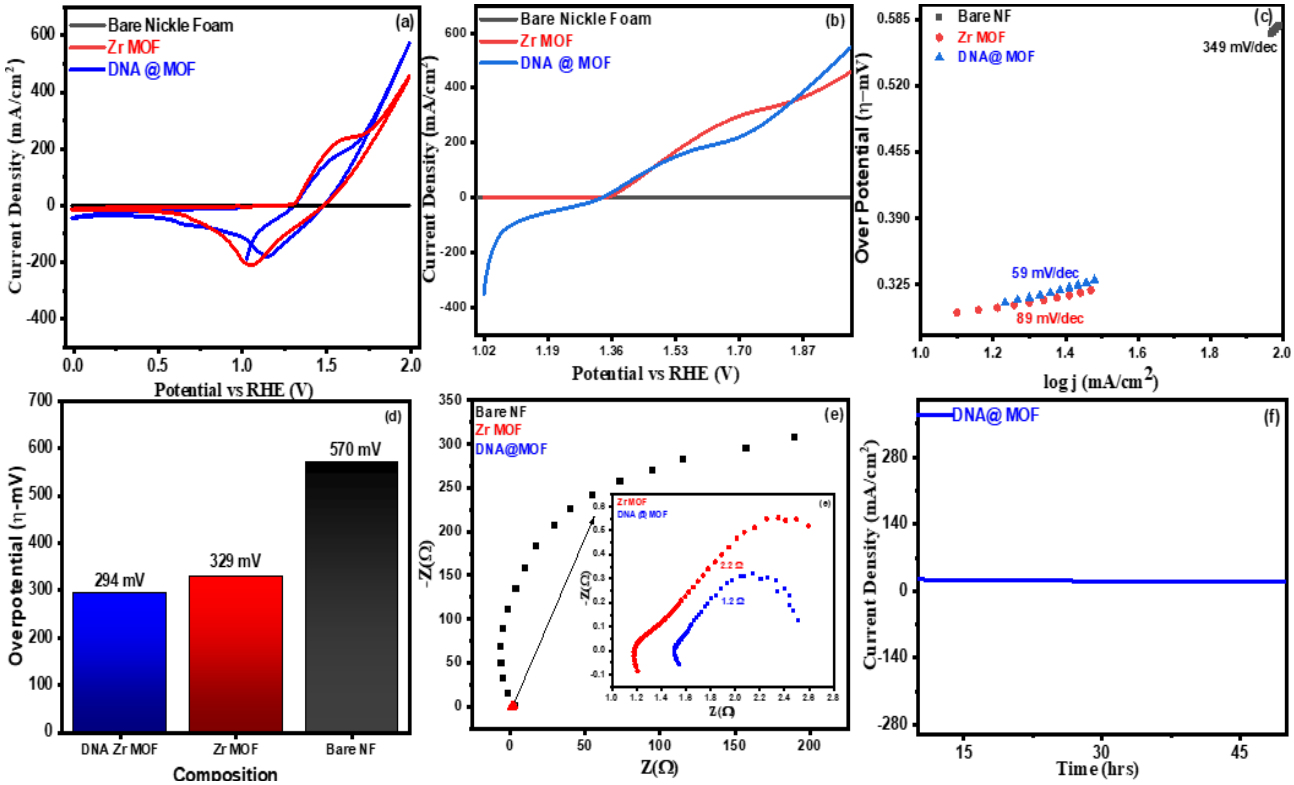

Fig. 6 a) CV Polarization Curves, b) LSV anodic linear scan, c) Tafel Plot, d) Overpotential Comparison, e) EIS analysis, f) Chronoamperometric stability test for elongated period of time

Structure of the porous framework depends mainly on organic linker which deeds as an essential building block to intersect the metal centers. In divergence to enclosure of the metal nodes, linker structure modification is another effective technique to modify the microelectronic arrangement of the active catalytic sites in MOFs to review their electro-chemical water splitting activities.

Electrochemical investigation was conducted on bare nickel foam (NF without catalyst loading), Zr-MOF and DNA encapsulated Zr-MOF. A bench mark current density of 10 $mAcm^{-2}$ is required to attain 10% efficiency in the solar-to-fuel conversion systems. (Gao *et al.* 2021) This value was used as a benchmark to evaluate the electro-catalytic efficacy of the prepared materials. Electrochemical

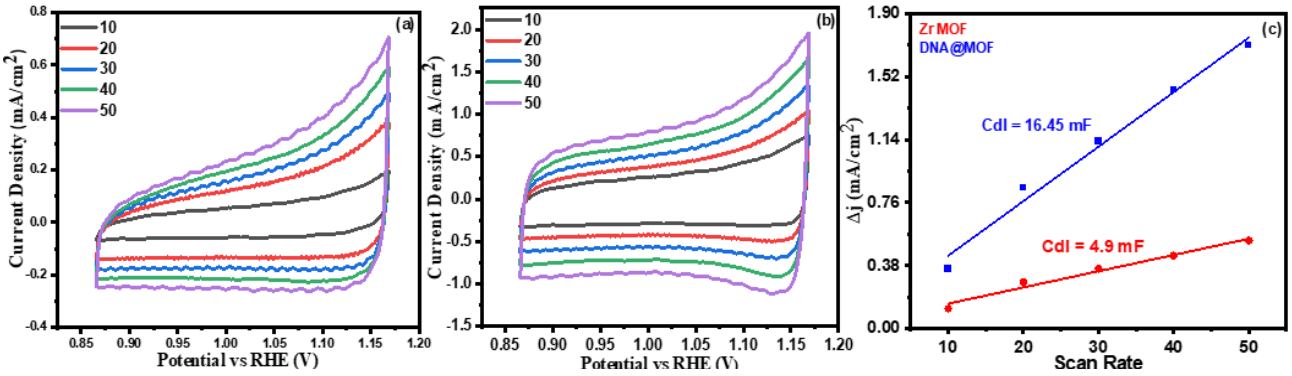

Fig. 7 Non-Faradaic region of CV polarization curves; (a) Zr-MOF, (b) DNA encapsulated Zr-MOF and (c) double layer capacitance slope calculated (Zr-MOF, DNA encapsulated Zr-MOF)

tests using CV polarization analysis as depicted in figure 6a revealed that the DNA encapsulated Zr-MOF has superior electro-chemical performance with a larger current density compared to Zr-MOF and Bare NF. Anodic linear scan was performed on the materials depicted in Fig. 6b. The onset potential was defined as follows: Bare NF had an onset potential of 1.71V, Zr-MOF had an onset potential of 1.62V and DNA encapsulated Zr-MOF showed an earlier onset potential of 1.49V due to the strong synergy between DNA and Zr-MOF. The DNA encapsulated Zr-MOF material exhibited a reduced overpotential of 294 mV compared to Zr-MOF (329 mV) and Bare NF (570 mV) to reach a standard 10 mA/cm^{2}current density, as illustrated in Fig. 6d.

Tafel slope tests were done to investigate the electro-catalytic activity of the Zr-MOF and DNA encapsulated Zr-MOF by examining the electrochemical kinetics of the slow OER. All these tests were conducted in linear area of the steady state polarization curve. The Tafel slope values are 349 mVdec^{-1} for bare NF, 89 mVdec^{-1} for Zr MOF and 59 mVdec^{-1} for DNA encapsulated Zr-MOF as illustrated in figure 6c. The DNA encapsulated Zr-MOF Tafel slope value was superior to that of many previously reported MOF-based electro-catalysts and was similar to the leading materials for OER such as 80 mV dec^{-1} for IrO_2 and 92.7 mV dec^{-1} for RuO_2@NF. This decreased value provided additional confirmation of the efficient and rapid transport of electrons and protons at the interfaces between the electrode and electro-catalyst. The Tafel slope value of 59 mVdec^{-1} indicates that the mechanism for Oxygen Evolution Reaction is proton-coupled electron transfer (PCET) (Weinberg *et al*. 2012). Throughout this process, the oxidation of single electron occurs simultaneously with the transfer of single proton. A rapid and early transfer of electrons during electrocatalysis results in higher catalyst efficiency and a lower Tafel slope. OER typically involves creation of hydroxyl ion (OH^-) intermediates and follows a 4-step proton-electron transfer pathway as depicted in Eqs. (1) to (4).

$$OH^- + Zr \rightarrow ZrOH + e^- \quad (1)$$

$$OH^- + ZrOH \rightarrow H^+ + ZrO + e^- \quad (2)$$

$$OH^- + ZrO \rightarrow ZrOOH + e^- \quad (3)$$

$$OH^- + ZrOOH \rightarrow Zr + O_2(g) + H^+ + e^- \quad (4)$$

Overall reaction: $4OH^- \rightarrow 2H_2O + 4e^- + O_2$

Currently, there are two commonly predictable OER methods; Lattice Oxygen-mediated Mechanism (LOM) and Adsorbate Evolution Mechanism (AEM). There are tranquil two divergent ways by which the oxygen is formed in the alkaline medium because catalytic centers first interact with the OH to form predecessors MO (M = Zr) and MOH. AEM is four electron methods wherever diverse intermediates (MOOOH, MOO and MOH) react to yield an O_2 as shown in Fig. 8. Entirely of these facts presented above your head favored outstanding collaboration of the electrocatalyst-electrolyte contacts for the duration of OER.

Aside from the Tafel slope, Electrochemical Impedance Spectroscopy (EIS) was conducted in frequency range of 10^5-0.1 Hz with varying current amplitude of 5 mV to clarify the charge transfer kinetics process. A small semicircle diameter of DNA encapsulated Zr-MOF is visible on the Nyquist plot in figure 6e indicating the lowest charge transfer resistance (Rct) of 1.2 Ω at the electro-catalyst-electrolyte interface compared to Zr MOF (Rct) of 2.2 Ω and bare NF (Rct) of 9.4 Ω. The lower Rct value and smaller semicircle diameter of the DNA@MOF compared to Zr-MOF and NF indicate a quicker electron transport. The data showed that adding DNA to MOF significantly improved the conductivity of the DNA encapsulated Zr-MOF and reduced resistance facilitating maximum electron transmission.

Material physical and chemical stability is crucial for evaluating electrochemical performance and long-term stability leads to the potential for high-performance devices. The stability of the produced samples was assessed using an elongated chronoamperometric stability test. The test showed that DNA encapsulated Zr-MOF shown exceptional stability, maintaining consistent performance without any decline for 50 hours as shown in Fig. 6f. This has the potential to be a dependable energy conversion technique.

Integrating DNA into MOF significantly decreased resistance, enhanced conductance and notably increased the active Electrochemical Surface Area (ECSA) of the DNA encapsulated Zr-MOF. Electrochemical surface area was determined for Zr-MOF and DNA encapsulated Zr-MOF by analyzing the non-faradaic portion of Cyclic Voltammetry

Table 1 Evaluation of electrochemical demonstration of various electrocatalysts

S. No.	Electrocatalysts	Over potential (mV) (η) at 10 mA/cm^2	Tafel slope (mV/dec)	Stability CV/LSV cycles	Chrono-amperometery (hrs)	Ref.
1	3D-CNTA	360	89	3,000	11.11	(Wang *et al*. 2017)
2	NiCoOS	470	--	800	--	(Bai *et al*. 2019)
3	Co-NC@Mo_2C	347	61	1,000	20	(Hossain. 2023)
4	MOF derived ZnCoSe	340	43	--	--	(Liang *et al*. 2022)
5	CoP/rGO	340	66	3,000	22	(Lu *et al*. 2021)
6	CDs@MOF	320	62	1,000	40	(Ahmed Malik *et al*. 2022)
7	Co/Co_9S_8@NSOC$_{800}$	373	80	--	10	(Du *et al*. 2019)
8	DNA encapsulated Zr-MOF	294	59	--	50	Current work

(CV) curves as shown in Fig. 7(a, b). The analysis resulted in delta j values displayed against scan rate which were used to calculate the slope value by linear regression to determine the double layer capacitance. The Electrical Double layered Capacitance (Cdl) value for Zr-MOF was determined to be 4.9 mF while for DNA encapsulated Zr-MOF it was 16.45 mF. A larger Cdl value indicates a greater electrochemical surface area when divided by the specific capacitance of the substrate material (0.04 mF/cm^2) (7(c)). ECSA was calculated as 122.5 cm^2 and for DNA encapsulated Zr-MOF it was 411.25 cm^2. Increased active surface area leads to greater adsorption of active substances onto the electrode's surface.

Higher surface area led to improved electrochemical performance and water splitting. DNA encapsulated Zr-MOF shows improved performance due to lower Tefol, reduced over potential of 294 mV and decreased resistance of 1.2 Ω resulting in superior electrochemical performance.

3.3 Durability of Zr-MOF and DNA encapsulated Zr-MOF electrocatalyst after OER

PXRD analysis has also been carried on the Zr-MOF and DNA encapsulated Zr-MOF material collected after the water splitting and this gave a conclusive proof that the structure of the MOFs is well maintained. Analysing the PXRD patterns obtained before and after OER reaction, it can be concluded that MOFs as well as DNA encapsulated Zr-MOF exhibit very high chemical stability. The results showed that the Zr-MOF and DNA encapsulated Zr-MOF are robust and have long-lasting amenity in facilitating sustainable and efficient electro-catalysis.

3.4 Comparison of Zr-MOF and DNA encapsulated Zr-MOF OER activity with other reported electro-catalysts

Analyzing the detailed literature data about electro-catalyst for OER, one can state that Zr MOF and DNA encapsulated Zr-MOF are exceptionally better than the other material to act as an electro-catalyst for the process of electrochemical water splitting. This gives an efficiently low overpotential (η) of 294 mV at 10 mA/cm² current density and much better than the performances of NiCoOS (470 mV), Co-NC@Mo_2C (347 mV) and CDs@MOF (320 mV). This lower overpotential is indicative of the high efficiency of ZrMOF and DNA encapsulated Zr-MOF in the catalysis of the electrochemical reaction; this implies that less energy will be used during operation which means lower operational costs. In addition, the Tafel values of the Zr-MOF and DNA encapsulated Zr-MOF are found to be 89 mV/dec and 59 mV/dec respectively that is relatively lesser than many of its counterparts and signifies for higher reaction kinetics. This characteristic is especially important to increase the performance of a reaction in terms of conversion rate and reaction rate in practice.

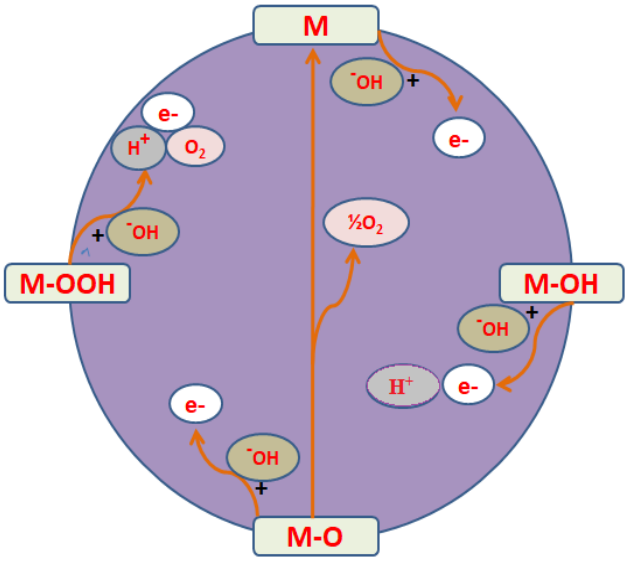

Fig. 8 Proposed mechanism for the OER catalyzed by Zr-MOF

As much as endurance is concerned, Zr-MOF and DNA encapsulated Zr-MOF again shows a long term chronoamperometric stability which lasts up to 50 hours and this greatly exceed the other catalysts given in table 1. Such a stability guarantees longer and stable operation under severe electrochemical processes and thus enhances its suitability of the material in industries and research. These attributes show the promising role of Zr-MOF and DNA encapsulated Zr-MOF for the advancement of electrocatalysis technology and more efficiency, economical and reliable in all the electrochemical processes.

4. Conclusion

In Summary, DNA encapsulated Zr-MOF and Zr-MOF (Zr-based single linker MOF) containing fumaric were successfully synthesized using a solvothermal process and investigated for their electrocatalytic performance in OER. The DNA encapsulated Zr-MOF exhibited a lower onset potential of 1.49 V relative to RHE for the OER and an overpotential of 294 mV vs. RHE that shows better results as associated to other advanced Metal Organic based electro-catalysts. Thus, when the DNA encapsulated Zr-MOF was run for a stability test over a long period of time *i.e.*, 50 h, it was found to have stability with a little decay in comparison with the initial values attained. Additionally, it achieved a high electrochemical surface area (ECSA) of 411.25 per cm^2 and a small charge transfer resistance of 1.2 Ω and small Tafel slope 59 mV dec^{-1}. Due to all these exceptional parameters, our DNA encapsulated Zr-MOF material was a best option for harnessing the earth's richest resource water for power generation.

Acknowledgement

Authors are very indebted to the Institute of Chemical Sciences for providing the research facilities at Bahauddin Zakariya University, Multan. Authors appreciatively acknowledge the State Key Laboratory of Advanced Technology for Materials Synthesis and Processing; Center for Chemical and Material Engineering, Wuhan University of Technology, Wuhan (430070), P. R. China.

References

Abazari, R., Amani-Ghadim, A.R., Slawin, A.M., Carpenter-Warren, C. L.and Kirillov, A.M. (2022), "Noncalcinedlayer-pillared $Mn_{0.5}Zn_{0.5}$ bimetallic-organic framework as a promising electrocatalyst for oxygen evolution reaction", *Inorg. Chem.*, **61**(25), 9514-9522. https://doi.org/10.1021/acs.inorgchem .2c00542

Abdelkareem, M.A., Elsaid, K., Wilberforce, T., Kamil, M., Sayed, E.T. and Olabi, A. (2021), "Environmental aspects of fuel cells: A review", *Sci. Total Env.*, **752**, 141803. https://doi.org/10.1016/j.scitotenv.2020.141803

Abdin, Z., Zafaranloo, A., Rafiee, A., Mérida, W., Lipinski, W. and Khalilpour, K. R. (2020), "Hydrogen as an energy vector", *Renew. Sust. Energy Rev.*, **120**, 109620. https://doi.org/10.1016/j.rser.2019.109620

Acar, C., Dincer, I. and Naterer, G. F. (2016), "Review of photocatalytic water-splitting methods for sustainable hydrogen production", *Int. J. Energy Res.*, **40**(11), 1449-1473. https://doi.org/10.1002/er.3549

Aghajani Hashjin, M., Zarshad, S., Motejadded Emrooz, H.B. and Sadeghzadeh, S. (2023), "Enhanced atmospheric water harvesting efficiency through green-synthesized MOF-801: A comparative study with solvothermal synthesis", *Sci. Rep.*, **13**(1), 16983. https://doi.org/10.1038/s41598-023-44367-1

Ahmed Malik, W.M., Afaq, S., Mahmood, A., Niu, L., Yousaf ur Rehman, M., Ibrahim, M., Mohyuddin, A., Qureshi, A.M., Ashiq, M.N. and Chughtai, A.H. (2022), "A facile synthesis of CeO_2 from the GO@Ce-MOF precursor and its efficient performance in the oxygen evolution reaction", *Front. Chem.*, **10**, 996560. https://doi.org/10.3389/fchem.2022.996560

Amaro-Gahete, J., Klee, R., Esquivel, D., Ruiz, J.R., Jimenez-Sanchidrian, C. and Romero-Salguero, F.J. (2019), "Fast ultrasound-assisted synthesis of highly crystalline MIL-88A particles and their application as ethylene adsorbents", *Ultrason. Sonochem.*, **50**, 59-66. https://doi.org/10.1016/j.ultsonch.2018.08.027

Baburin, I., Leoni, S. and Seifert, G. (2008), "Enumeration of not-yet-synthesized zeolitic zinc imidazolate MOF networks: a topological and DFT approach", *J. Phys. Chem. B.*, **112**(31), 9437-9443. https://doi.org/10.1021/jp801681w

Bai, Z., Li, S., Fu, J., Zhang, Q., Chang, F., Yang, L., Lu, J. and Chen, Z. (2019), "Metal-organic framework-derived Nickel Cobalt oxysulfide nanocages as trifunctional electrocatalysts for high efficiency power to hydrogen", *Nano Energy.*, **58**, 680-686. https://doi.org/10.1016/j.nanoen.2019.01.050

Banyay, M., Sarkar, M. and Graslund, A. (2003), "A library of IR bands of nucleic acids in solution", *Biophys. Chem.*, **104**(2), 477-488. https://doi.org/10.1016/S0301-4622(03)00035-8

Barman, B.K. and Nanda, K.K. (2016), "A noble and single source precursor for the synthesis of metal-rich sulphides embedded in an N-doped carbon framework for highly active OER electrocatalysts", *Dalton Trans.*, **45**(15), 6352-6356. https://doi.org/10.1039/C6DT00536E

Bennett, T.D. and Cheetham, A.K. (2014), "Amorphous metal-organic frameworks", *Acc. Chem. Res.*, **47**(5), 1555-1562. https://doi.org/10.1021/ar5000314

Bonnett, B.L., Smith, E.D., De La Garza, M., Cai, M., Haag IV, J.V., Serrano, J.M., Cornell, H.D., Gibbons, B., Martin, S.M. and Morris, A.J. (2020), "PCN-222 metal-organic framework nano-particles with tunable pore size for nanocomposite reverse osmosis membranes", *ACS Appl. Mater. Interf.*, **12**(13), 15765-15773. https://doi.org/10.1021/acsami.0c04349

Butova, V.V., Burachevskaya, O.A., Ozhogin, I.V., Borodkin, G.S., Starikov, A.G., Bordiga, S., Damin, A., Lillerud, K.P. and Soldatov, A.V. (2020), "UiO-66 type MOFs with mixed-linkers-1, 4-Benzenedicarboxylate and 1,4-naphthalenedicarboxylate: Effect of the modulator and post-synthetic exchange", *Micropor. Mesopor. Mater.*, **305**, 110324. https://doi.org/10.1016/j.micromeso.2020.110324

Butova, V.V., Pankin, I.A., Burachevskaya, O.A., Vetlitsyna-Novikova, K.S. and Soldatov, A.V. (2021), "New fast synthesis of MOF-801 for water and hydrogen storage: Modulator effect and recycling options", *Inorg Chim Acta.*, **514**, 120025. https://doi.org/10.1016/j.ica.2020.120025

Cai, G., Yan, P., Zhang, L., Zhou, H.C. and Jiang, H.L. (2021), "Metal-organic framework-based hierarchically porous materials: synthesis and applications", *Chem. Rev.*, **121**(20), 12278-12326. https://doi.org/10.1021/acs.chemrev.1c00243

Cavaliere, P. (2023), *Thermochemical Water Splitting Cycles In Water Electrolysis for Hydrogen Production*, Springer, Cham., 105-157, Lecce, Italy. https://doi.org/10.1007/978-3-031-37780-8_3

Cui, Y., Li, B., He, H., Zhou, W., Chen, B. and Qian, G. (2016), "Metal-organic frameworks as platforms for functional materials", *Acc. Chem. Res.*, **49**(3), 483-493. https://doi.org/10.1021/acs.accounts.5b00530

Dash, M., Chiellini, F., Ottenbrite, R.M. and Chiellini, E. (2011), "Chitosan-A versatile semi-synthetic polymer in biomedical applications", *Prog. Polym. Sci.*, **36**(8), 981-1014. https://doi.org/10.1016/j.progpolymsci.2011.02.001

Deng, H., Grunder, S., Cordova, K.E., Valente, C., Furukawa, H., Hmadeh, M., Gandara, F., Whalley, A.C., Liu, Z. and Asahina, S. (2012), "Large-pore apertures in a series of metal-organic frameworks", *Science.*, **336**(6084), 1018-1023. https://doi.org/10.1126/science.1220131

Dhaka, S., Kumar, R., Deep, A., Kurade, M.B., Ji, S.W. and Jeon,

B.H. (2019), "Metal-organic frameworks (MOFs) for the removal of emerging contaminants from aquatic environments", *Coord. Chem. Rev.*, **380**, 330-352. https://doi.org/10.1016/j.ccr.2018.10.003

Ding, M., Cai, X. and Jiang, H.L. (2019), "Improving MOF stability: Approaches and applications", *Chem. Sci.*, **10**(44), 10209-10230. https://doi.org/10.1039/C9SC03916C

Doorley, G.W., McGovern, D.A., George, M.W., Towrie, M., Parker, A.W., Kelly, J.M. and Quinn, S.J. (2009), "Picosecond transient infrared study of the ultrafast deactivation processes of electronically excited B-DNA and Z-DNA forms of [poly(dG-dC)]$_2$", *Angew. Chem. Int. Ed.*, **121**(1), 129-133. https://doi.org/10.1002/ange.200803904

Du, J., Wang, R., Lv, Y.R., Wei, Y.L. and Zang, S.Q. (2019), "One-step MOF-derived Co/Co_9S_8 nanoparticles embedded in nitrogen, sulfur and oxygen ternary-doped porous carbon: an efficient electrocatalyst for overall water splitting", *Chem. Comm.*, **55**(22), 3203-3206. https://doi.org/10.1039/C9CC00196D

Du, Y., Fang, H. X., Zhang, Q., Zhang, H. L. and Hong, Z. (2016), "Spectroscopic investigation on cocrystal formation between adenine and fumaric acid based on infrared and Raman techniques", *Spectrochim. Acta A Mol. Biomol. Spectrosc.*, **153**, 580-585. https://doi.org/10.1016/j.saa.2015.09.020

El Hankari, S., Bousmina, M. and El Kadib, A. (2019), "Biopolymer @metal-organic framework hybrid materials: A critical survey", *Prog. Polym. Sci.*, **106**, 100579. https://doi.org/10.1016/j.pmatsci.2019.100579

Falsafi, M., Saljooghi, A.S., Abnous, K., Taghdisi, S.M., Ramezani, M. and Alibolandi, M. (2021), "Smart metal organic frameworks: Focus on cancer treatment", *Biomater. Sci.*, **9**(5), 1503-1529. https://doi.org/10.1039/D0BM01839B

Farha, O.K., Eryazici, I., Jeong, N.C., Hauser, B.G., Wilmer, C.E., Sarjeant, A.A., Snurr, R.Q., Nguyen, S.T., Yazaydın, A.O. and Hupp, J.T. (2012), "Metal-organic framework materials with ultrahigh surface areas: is the sky the limit", *J. Am. Chem. Soc.*, **134**(36), 15016-15021. https://doi.org/10.1021/ja3055639

Francioso, O., Rodriguez-Estrada, M.T., Montecchio, D., Salomoni, C., Caputo, A. and Palenzona, D. (2010), "Chemical characterization of municipal wastewater sludges produced by two-phase anaerobic digestion for biogas production", *J. Hazard. Mater.*, **175**(1-3), 740-746. https://doi.org/10.1016/j.jhazmat.2009.10.071

Furukawa, H., Gándara, F., Zhang, Y.B., Jiang, J., Queen, W.L., Hudson, M.R. and Yaghi, O.M. (2014), "Water adsorption in porous metal-organic frameworks and related materials", *J. Am. Chem. Soc.*, **136**(11), 4369-4381. https://doi.org/10.1021/ja500330a

Furukawa, H., Go, Y. B., Ko, N., Park, Y.K., Uribe-Romo, F.J., Kim, J., O'Keeffe, M. and Yaghi, O.M. (2011), "Isoreticular expansion of metal-organic frameworks with triangular and square building units and the lowest calculated density for porous crystals", *Inorg. Chem.*, **50**(18), 9147-9152. https://doi.org/10.1021/ic201376t

Gao, D., Chen, J.H., Fang, S., Ma, T., Qiu, X.H., Ma, J.G., Gu, Q. and Cheng, P. (2021), "Simultaneous quantitative recognition of all purines including N6-methyladenine via the host-guest interactions on a Mn-MOF", *Matter.*, **4**(3), 1001-1016. https://doi.org/10.1016/j.matt.2020.12.016

Gao, Y., Julião, D., Silva, D.F., de Castro, B., Zhao, J. and Balula, S.S. (2021), "A simple desulfurization process to achieve high efficiency, sustainability and cost-effectivity via peroxotungstate catalyst", *Mol. Catal.*, **505**, 111515. https://doi.org/10.1016/j.mcat.2021.111515

Gautam, J., Chanda, D., Meshesha, M.M., Jang, S.G. and Yang, B.L. (2023), "Heterointerface of vanadium telluride and zinc iron telluride nanosheets for highly efficient hydrogen production via water and urea electrolysis", *Chem. Eng. J.*, **467**, 143535. https://doi.org/10.1016/j.cej.2023.143535

Ghazi, Z.M., Rizvi, S.W.F., Shahid, W.M., Abdulhameed, A.M., Saleem, H. and Zaidi, S.J. (2022), "An overview of water desalination systems integrated with renewable energy sources", *Desalination.*, **542**, 116063. https://doi.org/10.1016/j.desal.2022.116063

Gulati, S., Vijayan, S., Kumar, S., Harikumar, B., Trivedi, M. and Varma, R.S. (2023), "Recent advances in the application of metal-organic frameworks (MOFs)-based nanocatalysts for direct conversion of carbon dioxide (CO_2) to value-added chemicals", *Coord. Chem. Rev.*, **474**, 214853. https://doi.org/10.1016/j.ccr.2022.214853

Habib, U., Ahmad, F., Awais, M., Naz, N., Aslam, M., Urooj, M., Moqeem, A., Tahseen, H., Waqar, A. and Sajid, M. (2023), "Sustainable catalysis: navigating challenges and embracing opportunities for a greener future", *J. Chem. Environ.*, **2**(2), 14-53. https://doi.org/10.56946/jce.v2i2.205

Hayat, A., Sohail, M., Ali, H., Taha, T., Qazi, H., Ur Rahman, N., Ajmal, Z., Kalam, A., Al-Sehemi, A.G. and Wageh, S. (2023), "Recent Advances and Future Perspectives of Metal-Based Electrocatalysts for Overall Electrochemical Water Splitting", *Chem. Rec.*, **23**(2), e202200149. https://doi.org/10.1002/tcr.202200149

Hossain, E. (2023), *Energy from the Sun*, In *The Sun, Energy, and Climate Change*", Springer, Cham., 123-187. Boise, Idaho, USA. https://doi.org/10.1007/978-3-031-22196-5_3

Hou, Q., Zhou, S., Wei, Y., Caro, J.R. and Wang, H. (2020), "Balancing the grain boundary structure and the framework flexibility through bimetallic Metal-Organic Framework (MOF) membranes for gas separation", *J. Am. Chem. Soc.*, **142**(21), 9582-9586. https://doi.org/10.1021/jacs.0c02181

Jahan, I., Islam, M.A., Rupam, T.H., Palash, M.L., Rocky, K.A. and Saha, B.B. (2022), "Enhanced water sorption onto bimetallic MOF-801 for energy conversion applications", *Sust. Mater. Tech.*, **32**, e00442. https://doi.org/10.1016/j.susmat.2022.e00442

Jones, G.A. and Warner, K.J. (2016), "The 21st century population-energy-climate nexus", *Energy Policy.*, **93**, 206-212. https://doi.org/10.1016/j.enpol.2016.02.044

Karthick, K., Anantharaj, S., Ede, S.R., Sankar, S.S., Kumaravel, S., Karmakar, A. and Kundu, S. (2020), "Developments in DNA metallization strategies for water splitting electrocatalysis: A review", *Adv. Colloid Interface Sci.*, **282**, 102205. https://doi.org/10.1016/j.cis.2020.102205

Kibsgaard, J., Tsai, C., Chan, K., Benck, J.D., Nørskov, J.K., Abild-Pedersen, F. and Jaramillo, T. F. (2015), "Designing an improved transition metal phosphide catalyst for hydrogen evolution using experimental and theoretical trends", *Energy Environ. Sci.*, **8**(10), 3022-3029. https://doi.org/10.1039/C5EE02179K

Kim, H., and Hong, C.S. (2021). MOF-74-type frameworks: Tunable pore environment and functionality through metal and ligand modification", *CrystEngComm.*, **23**(6), 1377-1387. https://doi.org/10.1039/D0CE01870H

Lamiel, C., Hussain, I., Rabiee, H., Ogunsakin, O.R. and Zhang, K. (2023), "Metal-organic framework-derived transition metal chalcogenides (S, Se, and Te): Challenges, recent progress, and future directions in electrochemical energy storage and conversion systems", *Coord. Chem. Rev.*, **480**, 215030. https://doi.org/10.1016/j.ccr.2023.215030

Lee, S., Lee, M.H., Yoo, K.S. and Song, S. (2022), "Assessment of MOF-801 synthesis for toluene adsorption by using design of experiment methodology", *Korean J. Chem. Eng.*, **39**(11), 3129-3137. https://doi.org/10.1007/s11814-022-1199-8

Liang, C., He, J., Zhang, Y., Zhang, W., Liu, C., Ma, X., Liu, Y. and Gu, J. (2022), "MOF-derived CoNi@C-silver nanowires/

cellulose nanofiber composite papers with excellent thermal management capability for outstanding electromagnetic interference shielding", *Compos. Sci. Technol*., **224**, 109445. https://doi.org/10.1016/j.compscitech.2022.109445

Liu, Y., Alessi, D., Owttrim, G., Kenney, J., Zhou, Q., Lalonde, S. and Konhauser, K. (2016), "Cell surface acid-base properties of the cyanobacterium Synechococcus: Influences of nitrogen source, growth phase and N: P ratios", *Geochim. Cosmochim. Acta*., **187**, 179-194. https://doi.org/10.1016/j.gca.2016.05.023

Long, J.R. and Yaghi, O.M. (2009), "The pervasive chemistry of metal-organic frameworks", *Chem. Soc. Rev*., **38**(5), 1213-1214. https://doi.org/10.1039/B903811F

Lu, H., Tournet, J., Dastafkan, K., Liu, Y., Ng, Y.H., Karuturi, S.K., Zhao, C. and Yin, Z. (2021), "Noble-metal-free multi-component nanointegration for sustainable energy conversion", *Chem. Rev*., **121**(17), 10271-10366. https://doi.org/10.1021/acs.chemrev.0c01328

Mady, M.M., Mohammed, W.A., El-Guendy, N.M. and Elsayed, A.A. (2011), "Interaction of DNA and polyethylenimine: Fourier-transform infrared (FTIR) and differential scanning calorimetry (DSC) studies", *Int. J. Phys. Sci*., **6**(32), 7328-7334. https://doi.org/10.5897/IJPS11.1005

Martínez, N.P., Isaacs, M. and Nanda, K.K. (2020), "Paired electrolysis for simultaneous generation of synthetic fuels and chemicals", *New J. Chem*., **44**(15), 5617-5637. https://doi.org/10.1039/C9NJ06133A

Masuk, N.I., Mostakim, K. and Kanka, S.D. (2021), "Performance and emission characteristic analysis of a gasoline engine utilizing different types of alternative fuels: A comprehensive review", *Energy Fuels*., **35**(6), 4644-4669. https://doi.org/10.1021/acs.energyfuels.0c04112

McHugh, P.J., Stergiou, A.D. and Symes, M.D. (2020), "Decoupled electrochemical water splitting: From fundamentals to applications", *Adv. Energy Mater*., **44**(10), 2002453. https://doi.org/10.1002/aenm.202002453

Megía, P.J., Vizcaíno, A.J., Calles, J.A. and Carrero, A. (2021), "Hydrogen production technologies: From fossil fuels toward renewable sources. A mini review", *Energy Fuels*., **35**(20), 16403-16415. https://doi.org/10.1021/acs.energyfuels.1c02501

Mergel, J., Carmo, M. and Fritz, D. (2013), *Status on technologies for hydrogen production by water electrolysis*, In *Transition To Renewable Energy Systems*, John Wiley & Sons, 423-450. https://doi.org/10.1002/9783527673872.ch22

Miras, H.N., Vilà-Nadal, L. and Cronin, L. (2014), "Polyoxometalate based open-frameworks (POM-OFs) ", *Chem. Soc. Rev*., **43**(16), 5679-5699. https://doi.org/10.1039/C4CS00097H

Mohammadpour, H., Cord-Ruwisch, R., Pivrikas, A. and Ho, G. (2021), "Utilisation of oxygen from water electrolysis-Assessment for wastewater treatment and aquaculture", *Chem. Eng. J*., **246**, 117008. https://doi.org/10.1016/j.ces.2021.117008

Morris, W., Briley, W.E., Auyeung, E., Cabezas, M.D. and Mirkin, C.A. (2014), "Nucleic acid-metal organic framework (MOF) nanoparticle conjugates", *J. Am. Chem. Soc*., **136**(20), 7261-7264. https://doi.org/10.1021/ja503215w

Nadar, S.S., Vaidya, L., Maurya, S. and Rathod, V.K. (2019), "Polysaccharide based metal organic frameworks (polysaccharide–MOF): A review", *Coord. Chem. Rev*., **396**, 1-21. https://doi.org/10.1016/j.ccr.2019.05.011

Nandiyanto, A.B.D. and Okuyama, K. (2011), "Progress in developing spray-drying methods for the production of controlled morphology particles: From the nanometer to submicrometer size ranges", *Adv. Powder Technol*., **22**(1), 1-19. https://doi.org/10.1016/j.apt.2010.09.011

Nemiwal, M., Gosu, V., Zhang, T.C. and Kumar, D.(2021), "Metal organic frameworks as electrocatalysts: Hydrogen evolution reactions and overall water splitting", *Int. J. Hydrogen Energy*., **46**(17), 10216-10238. https://doi.org/10.1016/j.ijhydene.2020.12.146

Pan, Y., Abazari, R., Tahir, B., Sanati, S., Zheng, Y., Tahir, M. and Gao, J. (2024), "Iron-based metal-organic frameworks and their derived materials for photocatalytic and photoelectrocatalytic reactions", *Coord. Chem. Rev*., **499**, 215538. https://doi.org/10.1016/j.ccr.2023.215538

Peng, S., Bie, B., Jia, H., Tang, H., Zhang, X., Sun, Y., Wei, Q., Wu, F., Yuan, Y. and Deng, H. (2020), "Efficient separation of nucleic acids with different secondary structures by Metal-Organic Frameworks", *J. Am. Chem. Soc*., **142**(11), 5049-5059. https://doi.org/10.1021/jacs.9b10936

Rahman, M.A., Kim, J.H. and Hossain, S. (2022), "Recent advances of energy storage technologies for grid: A comprehensive review", *Energy Storage*., **4**(6), e322. https://doi.org/10.1002/est2.322

Rameesha, L., Rana, D. and Nagendran, A. (2024), "Poly (vinylidene fluoride) ultrafiltration membranes tailored with zirconium-based MOF-801 for water treatment applications", *Polym. Int*., **73**(5), 368-377. https://doi.org/10.1002/pi.6607

Rodenas, T., Luz, I., Prieto, G., Seoane, B., Miro, H., Corma, A., Kapteijn, F., Llabres i Xamena, F.X. and Gascon, J. (2015), "Metal-organic framework nanosheets in polymer composite materials for gas separation", *Nat. Mater*., **14**(1), 48-55. https://doi.org/10.1038/nmat4113

Sava Gallis, D.F., Butler, K.S., Pearce, C.J., Valdez, N. and Rodriguez, M.A. (2022), "Programmable photoluminescence via intrinsic and DNA-fluorophore association in a mixed cluster heterometallic MOF", *ACS Appl. Mater. Interf.*, **14**(8), 10566-10576. https://doi.org/10.1021/acsami.1c24477

Sazali, N. (2020), "Emerging technologies by hydrogen: A review", *Int. J. Hydrogen Energy*., **45**(38), 18753-18771. https://doi.org/10.1016/j.ijhydene.2020.05.021

Shi, J., Li J., Liang A., Jiang Z. (2023), "Highly catalysis Zinc MOF-loaded nanogold coupled with aptamer to assay trace carbendazim by SERS", *Adv. Nano Res*., **14**(4), 313-327. https://doi.org/10.12989/anr.2023.14.4.313

Shin, S., Haaring, R., So, J., Choi, Y. and Lee, H. (2022), "Highly durable heterogeneous atomic catalysts", *Acc. Chem. Res*., **55**(10), 1372-1382. https://doi.org/10.1021/acs.accounts.1c00734

Szeberenyi, A., Rokicki, T. and Papp-Vary, A. (2022), "Examining the relationship between renewable energy and environmental awareness", *Energies*., **15**(19), 7082. https://doi.org/10.3390/en15197082

Tian, L., Li, Z., Xu, X. and Zhang, C. (2021), "Advances in noble metal (Ru, Rh, and Ir) doping for boosting water splitting electrocatalysis", *J. Mater. Chem. A*., **9**(23), 13459-13470. https://doi.org/10.1039/D1TA01108A

Védrine, J. C. (2017), " Heterogeneous catalysis on metal oxides", *Catalysts*., **7**(11), 341. https://doi.org/10.3390/catal7110341

Wang, H.S., Liu, H.L., Wang, K., Ding, Y., Xu, J.J., Xia, X.H. and Chen, H.Y. (2017), "Insight into the unique fluorescence quenching property of metal-organic frameworks upon DNA binding", *Anal. Chem*., **89**(21), 11366-11371. https://doi.org/10.1021/acs.analchem.7b02256

Wang, Q., and Astruc, D. (2019), "State of the art and prospects in metal-organic framework (MOF)-based and MOF-derived nanocatalysis", *Chem. Rev*., **120**(2), 1438-1511. https://doi.org/10.1021/acs.chemrev.9b00223

Wang, S., Qin, J., Meng, T. and Cao, M. (2017), "Metal-organic framework-induced construction of actiniae-like carbon nanotube assembly as advanced multifunctional electrocatalysts for overall water splitting and Zn-air batteries", *Nano Energy*., **39**, 626-638. https://doi.org/10.1016/j.nanoen.2017.07.043

Wang, T.C., Bury, W., Gómez-Gualdrón, D.A., Vermeulen, N.A., Mondloch, J.E., Deria, P., Zhang, K., Moghadam, P.Z., Sarjeant, A.A. and Snurr, R.Q. (2015), "Ultrahigh surface area zirconium

MOFs and insights into the applicability of the BET theory", *J. Am. Chem. Soc.*, **137**(10), 3585-3591. https://doi.org/10.1021/ja512973b

Weinberg, D.R., Gagliardi, C.J., Hull, J.F., Murphy, C.F., Kent, C.A., Westlake, B.C., Paul, A., Ess, D. H., McCafferty, D. G. and Meyer, T.J. (2012), "Proton-coupled electron transfer", *Chem. Rev.*, **112**(7), 4016-4093. https://doi.org/10.1021/cr200177j

Wißmann, G., Schaate, A., Lilienthal, S., Bremer, I., Schneider, A. M. and Behrens, P. (2012), "Modulated synthesis of Zr-fumarate MOF", *Micropor. Mesopor. Mater.*, **152**, 64-70. https://doi.org/10.1016/j.micromeso.2011.12.010

Wu, F., Ye, J., Cao, Y., Wang, Z., Miao, T. and Shi, Q. (2020), "Recent advances in fluorescence sensors based on DNA–MOF hybrids", *Luminescence.*, **35**(4), 440-446. https://doi.org/10.1002/bio.3790

Wu, J., Dai, Q., Zhang, H. and Li, X. (2021), "A defect-free MOF composite membrane prepared via in-situ binder-controlled restrained second-growth method for energy storage device", *Energy Stor. Mater.*, **35**, 687-694. https://doi.org/10.1016/j.ensm.2020.11.040

Wu, Y., Liu, J., Sun, Q., Chen, J., Zhu, X., Abazari, R., and Qian, J. (2024), "Molecular catalyst of Fe phthalocyanine loaded into in-based MOF-derived defective carbon nanoflowers for oxygen reduction", *Chem. Eng. J.*, 149243. https://doi.org/10.1016/j.cej.2024.149243

Yuan, S., Chen, Y.P., Qin, J., Lu, W., Wang, X., Zhang, Q., Bosch, M., Liu, T.F., Lian, X. and Zhou, H.C. (2015), "Cooperative cluster metalation and ligand migration in zirconium metal-organic frameworks", *Angew. Chem. Int. Ed.*, **54**(49), 14696-14700. https://doi.org/10.1002/anie.201505625

Zhang, B., Zheng, Y., Ma, T., Yang, C., Peng, Y., Zhou, Z., Zhou, M., Li, S., Wang, Y. and Cheng, C. (2021), "Designing MOF nanoarchitectures for electrochemical water splitting", *Adv. Mater.*, **33**(17), 2006042. https://doi.org/10.1002/adma.202006042

Zhang, X., Chen, Z., Liu, X., Hanna, S.L., Wang, X., Taheri-Ledari, R., Maleki, A., Li, P. and Farha, O.K. (2020), "A historical overview of the activation and porosity of metal-organic frameworks", *Chem. Soc. Rev.*, **49**(20), 7406-7427. https://doi.org/10.1039/D0CS00997K

Graphical Abstract